

High resolution observations of the ocean upper layer south of Cape São Vicente, western northern margin of the Gulf of Cadiz.

Sarah A. Rautenbach³, Carlos Mendes de Sousa^{1,2}, Mafalda Carapuço⁴, Paulo Relvas¹

1 Centre of Marine Sciences (CCMAR), University of Algarve, Faro, Portugal

2 Portuguese Institute for the Sea and Atmosphere (IPMA, I.P.), Lisboa, Portugal

3 Deltares, Delft, The Netherlands

4 Atlantic International Research Centre, Azores, Portugal

Abstract

This article presents an Eulerian physical and biogeochemical data set from the Iberian Margin Cape São Vicente Ocean Observatory (IbMa-CSV), a facility of the European Multidisciplinary Seafloor and water column Observatory - European Research Infrastructure Consortium (EMSO-ERIC) located 10 nautical miles south of Cape São Vicente (Portugal), the southwest tip of the Iberian Peninsula and western limit of the northern margin of the Gulf of Cadiz. The observatory was installed on the shelf break, and the data time series spans four months for most of the variables. The upper 150 m were sampled intensively with a wave powered vertical profiler at an average rate of 4.5 profiles per hour recording at 2 Hz when ascending at approximate velocity of 0.2 m/s and 10 Hz when descending at variable velocity. The vertical resolution was always higher than 0.2 m. Measured channels were conductivity, temperature, pressure, chlorophyll *a*, dissolved O₂ concentration, and turbidity. Derived channels are sea pressure, depth, salinity, speed of sound, specific conductivity, dissolved O₂ saturation, density anomaly, spiciness and Brunt-Väisälä frequency. The acquired data set includes the flow velocity and direction along the water column, taken from an upward looking 300 kHz Acoustic Doppler Current Profiler (ADCP) recorded every hour for 3 m depth bins extending the same depth range of the vertical profiler. A standard quality control scheme was applied to the data set. The data set is preserved for multiple use and is accessible in the Sea Open Scientific Data Publication (SEANOE) repository, under the address: <https://www.seanoe.org/data/00836/94769/> (Rautenbach et al., 2022).

Key words: High resolution dataset, vertical profiles, EMSO-ERIC, IbMa-CSV observatory, Cape São Vicente, Western Gulf of Cadiz

32 **1. Introduction: the relevance of the site's location**

33 The Iberian Peninsula (Figure 1) represents the northern branch of the Canary Current Upwelling System
34 (CCUS), one of the four Eastern Boundary Upwelling Systems (EBUS), along with the Benguela,
35 California and Humboldt or Peru upwelling systems. These systems are characterized by the coastal
36 upwelling of cold nutrient rich subsurface water, driven by the joint action of northerly winds that blow
37 at least during a substantial part of the year, and the Earth's rotation (Ekman mechanism). Therefore,
38 those systems are among the most productive of the world ocean, which justifies their socio-economic
39 relevance.

40 The CCUS is unique among the EBUS, since it is the only one punctuated by a discontinuity that is
41 imposed by the entrance of the Mediterranean Sea into the Gulf of Cadiz (GoC) through the Strait of
42 Gibraltar (Figure 1). The meridional coast of the western Iberian Peninsula is abruptly interrupted at the
43 Cape São Vicente (CSV), the southwestern tip of the Iberian Peninsula. There, the coastline turns almost
44 at a right angle into the zonal orientated northern margin of the GoC.

45 The continental shelf off the southern part of the western Iberia and in the CSV area is narrow (< 10 km
46 wide south of 38° N), approximately delimited by the 200 m bathymetric contour. Over the continental
47 shelf and slope, roughly from April to October, the oceanographic conditions are largely dominated by
48 the upwelling process and associated cold jet flowing equatorward (Relvas and Barton, 2002). For the
49 remainder of the year, the flow is expected to point northward, although there is a lack of observational
50 evidence. Nevertheless, there is measured evidence that over the inner shelf the upwelling pattern is
51 interrupted by the development of a warm coastal counter-current whenever the upwelling favorable
52 winds relax below a certain threshold (Relvas and Barton 2005; Garel et al., 2016).

53 The Coastal Transition Zone, defined as the region where the coastal waters interact with the offshore
54 oceanic waters, is populated by a variety of mesoscale structures, such as meanders, eddies, and
55 filaments. The CSV is the root of a recurrent upwelling filament that may extend more than 150 km
56 offshore (Sanchez et al., 2008), exporting to the open ocean a much larger mass than expected by the
57 purely wind-driven Ekman circulation. The new production of an upwelling season could be entirely
58 exported to the open ocean by upwelling filaments (Aristegui et al., 2006), revealing the importance of
59 such features to the ecosystem functioning.

60 At deeper levels, where the wind is not a forcing factor, the CSV region reveals fascinating processes
61 related to the Mediterranean Outflow Water (MOW). After leaping the shallow sill (< 300 m deep) of
62 the Strait of Gibraltar, the salty and warmer MOW sinks sharply into the deep GoC (depths up to 4000
63 m), and spreads at depths between 800 and 1200 m, where it finds the equilibrium in the gravitational
64 field (Sanchez et al, 2017). However, a shallow vein detaches and flows at depths as shallow as 400 m
65 or less along the northern continental slope of the GoC, turning poleward around the CSV (Ambar 1983;
66 Cardeira et al., 2013).

67 The higher level of salt entering the North Atlantic through the Strait of Gibraltar and how it spreads
68 throughout the Atlantic basin is a key factor with implications in the functioning of the Atlantic
69 Meridional Overturning Circulation (AMOC), and therefore with climatic consequences. Due to the
70 water column stability, diapycnal mixing of the MOW through entrainment occurs at long time scales
71 when compared with horizontal dispersion through advection (Mauritzen et al, 2001). MOW is
72 dominated by a succession of mesoscale rotating structures, the so called meddies (Mediterranean
73 eddies) (Bower et al., 1995; Ambar et al., 2008). Meddies are described as rotating salt-water lenses,
74 typically 50-200 km wide and 100-200 m thick. There is some evidence that the dynamic effect of
75 meddies propagate along the entire water column, till the surface (Serra et al, 2010). CSV is identified
76 as a site for meddy generation. Topographic features along the continental slope near CSV are
77 hypothesized as meddy triggers. The key role that the CSV region plays in a wide variety of
78 oceanographic processes of all scales, some impacting the entire North Atlantic circulation,
79 demonstrates the relevance of the region to install a high-resolution subsurface observatory.

80 **2. Motivation and Objectives**

81 In the frame of the European Multidisciplinary Seafloor and water column Observatory – European
82 Research Infrastructure Consortium (EMSO-ERIC – <https://emso.eu/>) physical and biogeochemical
83 data from fixed ocean observation platforms throughout Europe are aggregated, harmonized, and
84 shared openly under the Creative Commons Attribution License (CC-BY) license, guaranteeing open
85 access for anyone. EMSO-ERIC is a distributed research infrastructure, encompassing observatories
86 and test sites along European waters, from coastal to deep sea locations. Some observatories have
87 already been operating for some time, whereas other nodes are yet to be established.

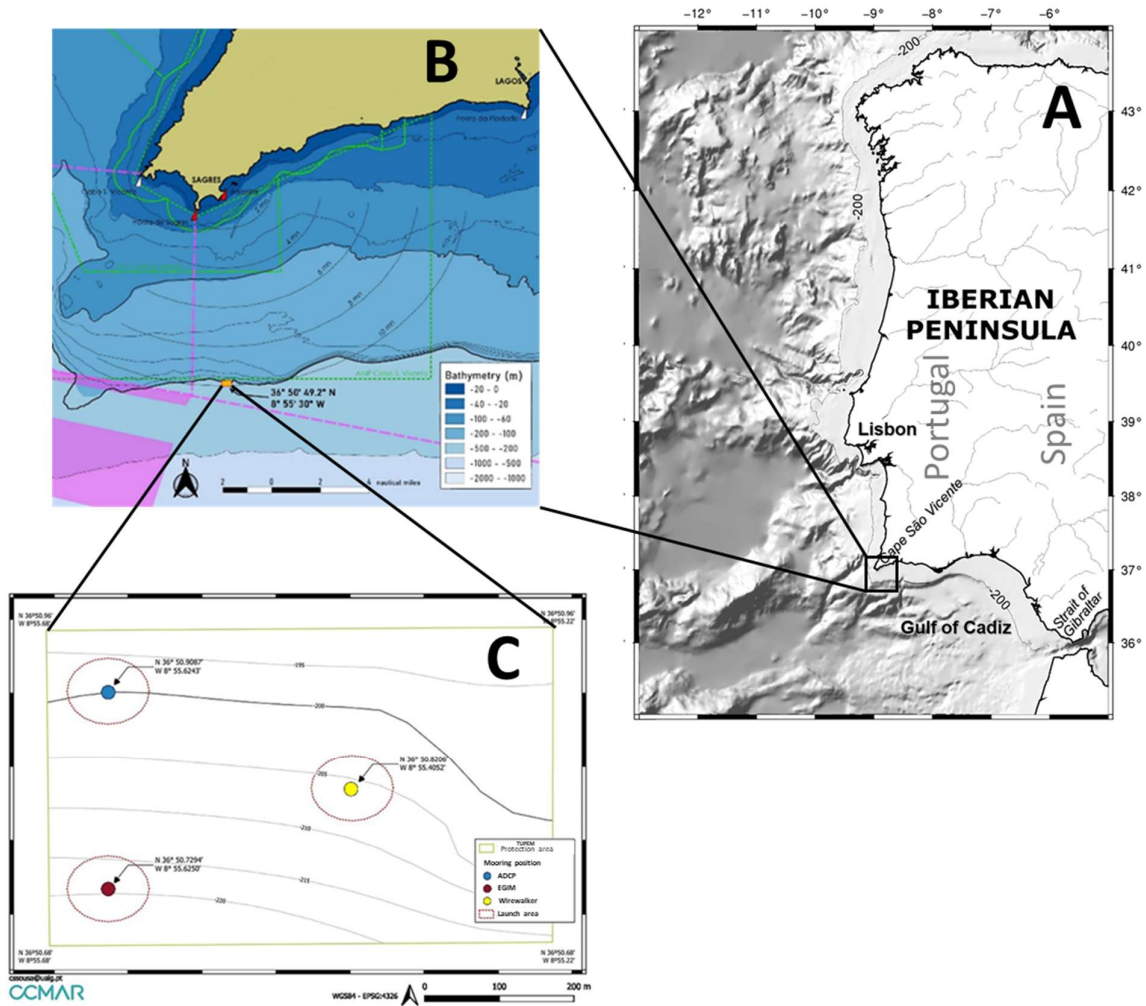
88 The EMSO-ERIC initiative defined the Iberian margin, specifically the region southwest of the CSV,
89 as the location to install a regional facility of its European network. Along with other objectives
90 related to geo-hazards seafloor observations, this was the opportunity to carry out long term *in situ*
91 observations of the subsurface ocean in a clearly under sampled area, regarding its oceanographic
92 relevance. In the region, *in situ* observations are limited to event scale records from research cruises.
93 Therefore, the main goal was to construct continuous high resolution and long-term time series of
94 oceanographic variables along the water column. A mobile platform carrying oceanographic sensors,
95 moving continuously throughout the water column, robust enough to survive the energetic seas of the
96 region for long periods, was carefully selected. The vertical definition of the flow field would be
97 ensured by placing an acoustic doppler current profiler (ADCP) nearby, sampling the entire water
98 column. The EMSO-Iberian Margin - Cape São Vicente observation platform (IbMa-CSV) is currently
99 producing the first long term set of observations, from which the seminal deployment data are
100 presented in this article.

101 While, *in situ* observations play a major role in understanding ocean dynamics and can be used for
102 various purposes, until today the availability of continuous and long-term *in situ* data of the ocean is
103 sparse. The construction of long high-resolution time-series is fundamental to access the long-term
104 physical and biogeochemical variability of the water column, and to improve modeling efforts, meeting
105 climatic change and ecosystem functions objectives. The data gathered are highly valuable for the
106 scientific community, with social and economic implications. Most political decisions are taken based
107 on evidence or future scenarios, mainly provided by numerical models. Due to the turbulent nature of
108 the ocean flow, numerical models need to be parametrized. More accurate parameterizations are
109 achieved when based on *in situ* observations, the higher the resolution the better, resulting in more
110 realistic numerical models. Therefore, one of the criteria that drove the choice of the observation devices
111 to install at IbMa-CSV was the generation of high-resolution records.

112 **3. Methods**

113 *3.1 The EMSO-Iberian Margin Cape São Vicente observatory (IbMa-CSV) - setup and operation*

114 The IbMa-CSV is located at the southwestern tip of the Iberian Margin, 10 nm south of CSV, on the
115 edge of the continental shelf (approximately 200 m depth). Deployment site selection carefully
116 considered fishing activity in the surrounding area, avoiding well known heavy equipment preferred
117 routes (e.g. trawling, longlines). A Permit for Private Use of the National Maritime Space (TUPEM)
118 was authorized by the Directorate-General for Natural Resources (DGRM) for an area of 0.35 km², in
119 which the observatory is deployed and should not be entered by other parties. However, ship traffic and
120 fishing activities pose a significant risk to the observatory as the TUPEM area is not patrolled. To
121 minimize this risk, engagement actions were undertaken with local communities and the legal
122 concession publicized in local navigation charts through official channels. This approach proved to be
123 successful as there was no visible and/or reported incident. The boundaries of the TUPEM area are
124 N36°50.9087' W8°55.6243', N36°50.9600' W8°55.2200', N36°50.6800' W8°55.6800' and
125 N36°50.6800' W8°55.2200'. Within this area the instruments are fixed on three separate moorings
126 (Figure 1C). The TUPEM is managed by the Algarve Centre of Marine Sciences (CCMAR), Faro,
127 Portugal.



128

129 **Figure 1.** Location of the CSV region (A). Reserved TUPEM , managed by the CCMAR. IbMa-CSV is located within the
 130 TUPEM area (B). Mooring sites for each platform; vertical wave-powered profiler (surface, yellow), EGIM (subsurface, red),
 131 ADCP (subsurface, blue) (C).

132 Mooring design followed current best practices (e.g. Coppola et al., 2016), based on two
 133 platform types: subsurface (EGIM and ADCP), and surface (vertical profiler; Figure 2). The
 134 subsurface moorings were conceived as linear structures from anchor to buoy, while the surface
 135 mooring was based on an inverse catenary configuration. The choice of the hardware to be used
 136 in the mooring, i.e. the size and shape of the anchor, the type of rope and chain, number, size
 137 and shape of flotation aids and their position along the mooring line, linking hardware (shackles,
 138 swivels, d-links), were all carefully considered to meet the environmental features of the
 139 deployment area (e.g. waves, atmospheric forcing, presence of strong currents). Static and
 140 dynamic behavior of all three designs was then simulated in a dedicated software (Proteus DS),
 141 considering time dependent forcing parameters (wind, currents and waves) to evaluate vertical
 142 load, components position, tilt and tension, required safe anchor mass, and overall mooring
 143 configuration, according to different set scenarios, i.e. “normal”, “storm”, and “extreme”.

144 Moorings were required not only to endure “extreme” conditions without failure, but also
145 maintain operational capabilities (to a reasonable extent) under more energetic events.
146 Simulated results pointed to neglectable instrumentation tilt of the subsurface moorings under
147 a set maximum 0.6 m/s current. Regarding the surface mooring, vertical travel wire inclinations
148 greater than 20° were expected to hinder vertical motion. Simulated inclinations were on
149 average 5.7°, 15.2°, and 29.5°, under “normal”, “storm” and “extreme” scenarios, respectively,
150 as such considered to be satisfactory. Operating depths, i.e. the subsurface platforms placed
151 broadly below 150 m depth, and the vertical profiler travelling between approximately 150 m
152 and 1 m in constant motion (~5 or 6 full profiles per hour), were expected to deter significant
153 biofouling growth, requiring as such minor control techniques, such as a homespun coating
154 applied to the ADCP transducers (zinc oxide paste mixed with cayenne pepper), as well as
155 copper tape around the optical sensors. Recovered equipment experienced, as expected,
156 biofouling, however, while the ADCP subsurface platforms were unaffected, the vertical
157 profiler was compromised after the two months, where algae growth led to the salinity sensor
158 operation hinderance. Based on these findings, a new strategy must be developed for future
159 deployments, whether it is to clean the sensors regularly during the deployment period or using
160 innovative biofouling control techniques compatible with available sensors (wipers, non-toxic
161 coating, UV lights, for instance)

162 *3.2 Data acquisition platforms and settings Instruments, parameters, and sampling*

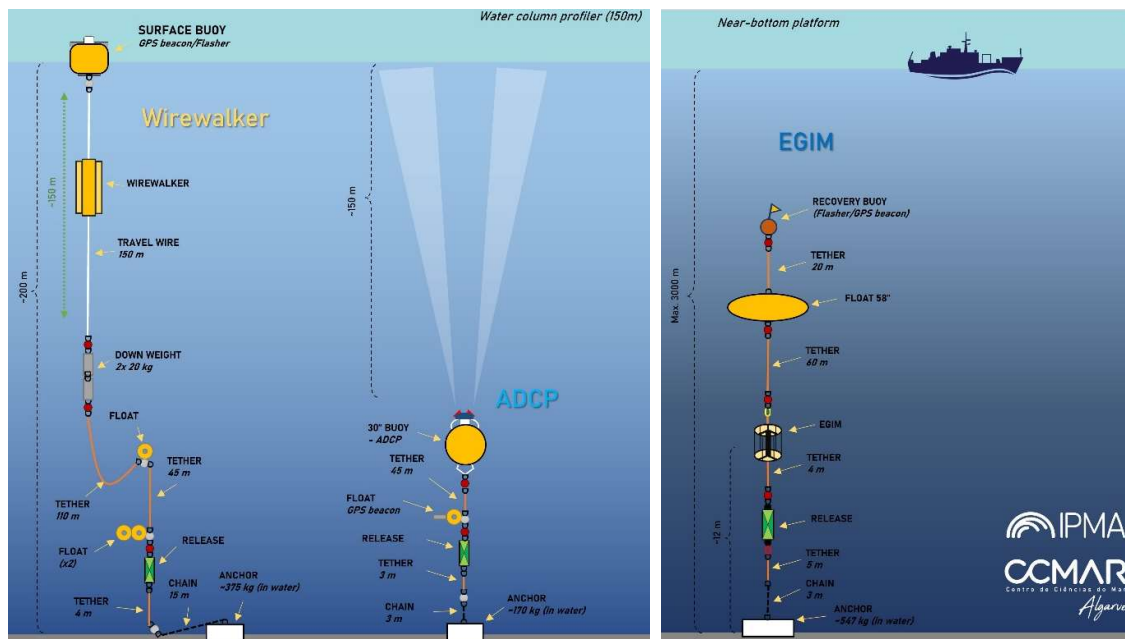
163 An ADCP (Teledyne RDI Sentinel V100 300 kHz), mounted in a upward facing subsurface buoy
164 (36.848478 N , -8.927072 E; 150 m), a vertical wave-powered profiler (Wirewalker) (36.84701 N, -
165 8.92342 E; near surface to 150 m), and an EMSO Generic Instrument Module (EGIM) (36.84549 N, -
166 8.927083 E; 200 m) were deployed from the R/V Mário Ruivo during the EMSO-PT Leg 2 Campaign,
167 in collaboration with the Portuguese Institute for the Sea and Atmosphere, I.P. (IPMA, I.P.), in the
168 TUPEM area during June – October 2022 (Figure 1C).

169 ADCP data were collected every hour for 3 m depth bins (51 bins in total), mounted at 150 m depth
170 (Figure 2). The blank right above the ADCP accounts for 2 m. Ping interval was 1 s and number of pings
171 120. East-west and north-south component (ms^{-1}) of the current together with the magnitude and
172 direction were acquired. Supplemental parameters, substantial for quality control, are provided
173 additionally, including correlation, echo intensity and percent of good return of each of the four beams,
174 as well as heading, pitch, and roll. The ADCP was further equipped with a thermistor and pressure
175 sensor. The ADCP was calibrated before the deployment according to manufacture guidelines.

176 A 6 channel RBRconcerto CTD, equipped with two Turner Designs Cyclops 7F sensors (Chl-a and
177 Turbidity) and one RBRcoda3 T.ODO (optical dissolved oxygen) were installed in a vertical wave-

178 powered vertical profiler, travelling from about 1 m below surface to 150 m depth at an variable speed:
 179 upward cast (free floating) $\sim 0.5 \text{ ms}^{-1}$; downward cast (wave motion) $\sim 0.4 \text{ ms}^{-1}$ (depending on wave
 180 conditions). Sampling rate was 2 Hz ascending, and 10 s descending. Measured channels were
 181 conductivity, temperature, pressure, chlorophyll-a, dissolved O_2 concentration, and turbidity. Derived
 182 channels are sea pressure, depth, salinity, speed of sound, specific conductivity, dissolved O_2 saturation,
 183 and density anomaly.

184 The EGIM, equipped with a SeaBird SBE37, Aanderaa 4831dw, RBRquartz 3 BPR, WETLabs ECO-
 185 NTU, OCEANSONICS icListen SB60L-ETH and Teledyne RDI 300kHz Workhorse Monitor direct-
 186 reading ADCP, was fixed at approximately 200 m depth.



187
 188 **Figure 2.** Schematic representation of the IbMa-CSV platforms. Left: Vertical wave-powered profiler and ADCP moorings,
 189 managed by CCMAR. Right: EGIM mooring, managed by IPMA and CCMAR.

190 Sampling period was 60 minutes (ADCP), 15 minutes (CT, Turbidity, Oxygen), 30 seconds (Pressure),
 191 and 5 minutes / 1 minute recording (acoustics). Measured channels include conductivity, temperature,
 192 pressure, temperature, dissolved O_2 concentration, turbidity, currents, and passive acoustics. Derived
 193 channels are sea pressure, depth, salinity, speed of sound, specific conductivity, dissolved O_2 saturation,
 194 and density anomaly. The data time-series from the ADCP and the Wirewalker, managed by CCMAR,
 195 will be presented in this data paper, along with the description of the data processing and results.

196 4. Data files and metadata

197 Instrument data files come in comma-separated value files and are converted into NetCDF format
 198 according to CF Conventions 1.6. Files are named after facility code, platform code (WW, EGIM),
 199 deployment number (D01, D02, ..., Dnn), deployment period, and version (v001, v002, ..., vnnn) e.g.
 200 [folder_path]IBMA-CSV_WW_D01_yyyymmdd_to_yyyymmdd_v001.nc. Changes are tracked in a

201 log-text file, which is located in the “dataset type” – directory. Instrument data (raw) are identified with
 202 the code “*_v001” and metadata with code “*_M”.

203 The vertical wave-powered profiler data are divided into six NetCDF files, each one approximately two
 204 million data points, to keep file size reasonable. Each NetCDF is built upon the same structure: Global
 205 attributes, Dimensions and Variables. Global attributes describe the dataset universally through a short
 206 descriptive summary as well as other attributes such as temporal extension, geospatial position, principal
 207 investigator, person of contact and more (Table 1). Each variable is embedded in one or more
 208 dimensions, in this case: Time, Longitude, Latitude, Depth and Bins. Each parameter is accompanied
 209 by a set of metadata attributes, holding detailed information about the instrument type, the units and
 210 other relevant information regarding the variable. The SeaDataNet parameter discovery vocabulary
 211 (<https://vocab.seadatanet.org/search>), well established in ocean science, is used for attributes,
 212 dimensions, variables and units. Further, vocabulary is based on the Copernicus Marine Environment
 213 Monitoring Service *In Situ* Thematic Assembly Centre (CMEMS INSTAC) Manual v3.2 and
 214 SeaDataNet OceanSITES Data Format Reference Manual v1.4. Common vocabulary facilitates
 215 machine-readability and manual findability by users. Each dataset is accompanied by comprehensive
 216 metadata. Global and variable specific metadata attributes were agreed upon in the Data Management
 217 Service Group (DMSG) of EMSO-ERIC (Table 1). The main objective of EMSO-ERIC DMSG is to
 218 make each dataset as findable, accessible, interoperable and (re)usable as possible, according to FAIR
 219 standards, harmonize data quality control, format and metadata procedures. Each in this data paper
 220 presented dataset can be reused under the CC-BY 4.0 license (<https://spdx.org/licenses/CC-BY-4.0>).

221 **Table 1.** EMSO-ERIC Data Management Service Group Metadata Catalogue.

Global Attributes	Dimensions	Variables	Quality Control
date_created	long_name	long_name	long_name
Conventions	standard_name	standard_name	flag_values
institution_edmo_code	units	units	flag_meanings
institution_edmo_uri	axis	comment	conventions
insituation_ror_uri	ancillary_variables	coordinates	
geospatial_lat_min	sdn_parameter_name	ancillary_variables	
geospatial_lat_max	sdn_parameter_urn	sdn_parameter_name	
geospatial_lon_min	sdn_uom_name	sdn_parameter_urn	
geospatial_lon_max	sdn_uom_urn	sdn_parameter_uri	
geospatial_vertical_min		reference_scale	
geospatial_vertical_max		sdn_uom_name	
time_coverage_start		sdn_uom_urn	
time_coverage_end		sdn_uom_uri	
update_interval		sensor_model	
site_code		sensor_reference	
emso_facility		sensor_type_uri	
source		sensor_type_name	

platform_code		sensor_manufacturer	
wmo_platform_code		sensor_manufacturer_uri	
data_type		sensor_serial_number	
format_version		sensor_mount	
network		sensor_orientation	
data_mode		sensor_depth	
title		QC_indicator	
summary			
keywords			
keywords_vocabulary			
project			
principal_investigator			
principal_investigator_email			
doi			
references			
license			
license_uri			

222

223 Quality control variables were created for each measured parameter and for some derived parameters.
 224 The quality control variable name is composed of the variable name of the parameter and the suffix
 225 “_QC”. Quality control procedures and flagging conventions are described in further detail in the next
 226 section. For each dataset it was assured that solely measurements conducted in the water column were
 227 considered. This was achieved by examining depth measurements, derived from the pressure sensor as
 228 well as temperatures indicating atmospheric temperatures. Out of water values were removed from each
 229 dataset.

230 **5. Technical Validation**

231 Each dataset was subject to quality control (qc). Suspicious and bad values were not removed from the
 232 published raw dataset. Instead, a complimentary qc-variable was created, holding flag values describing
 233 each individual parameter value. Flag values are defined by the OceanSITES Data Format Reference
 234 Manual v1.4 (OceanSITES, 2020). Flag may take the values 0, 1, 2, 3, 4, 7, 8, 9 that are defined as
 235 “unknown”, ”good_data”, “probably_good_data”, “potentially_correctable bad_data”, “bad_data”,
 236 “nominal_value”, “interpolated_value”, “missing_value”, respectively. Suspicious and bad values were
 237 flagged as “potentially_correctable bad_data” (3) and “bad_data” (4), respectively.

238 Contrary to the published raw dataset, this paper presents the quality controlled data. Data flagged as
 239 “potentially_correctable bad_data”, “bad_data” and “missing_value” were excluded from the plots
 240 presented in this manuscript.

241 ADCP quality control was based on the quality control procedures from Garel *et. al.* (2016). To ensure
 242 that no data subject to site lobe interference is shared, the upper 10 % of the data was flagged as

243 “bad_data”. Further, the sea surface was detected by locating the cells with a difference among adjacent
244 values greater than three and flagged bad accordingly. This criterion was restricted to cells above the
245 14th cell (100 m) to prevent misinterpretation of the surface. Cells above and the cell immediately below
246 were flagged as “bad_data”. Furthermore, if two or more beams with cells featuring a difference among
247 adjacent bins in echo intensity > 30, and/or with three or more out of four beams with correlation
248 magnitude values lower 64 counts were also flagged as “bad_data”. Temperature was controlled
249 according to SeaDataNet Guidelines (see above), and pressure was assessed via visual inspection.

250 The first quality control check for the vertical profiler data was done visually via line and boxplots of
251 each variable, allowing a global and regional range check and spike detection at first sight. Quality tests
252 applied on each variable of this dataset were: Sensor range test, global range test, regional range test and
253 spike test. A gradient test was additionally applied to temperature and salinity. Global ranges were
254 obtained from literature for each variable, whereas regional ranges were discussed and selected with the
255 support of experts from the region.

256 Temperature and salinity Spike Test (ST) was conducted according to SeaDataNet Data Quality Control
257 Procedures Manual (SeaDataNet 2010), using the following algorithm: Test value = $|V2 - (V3 + V1)/2$
258 $- | (V3 - V1) / 2 | > V$ THRESHOLD. The value is flagged “bad_data” when the test value exceeds
259 6 °C, 0.9 PSU, respectively. Gradient Test (GT) relied on the following from SeaDataNet proposed
260 algorithm: Test value = $(|V2 - (V1 + V3)/2| > V$ _GRAD. The value is flagged “bad_data” when the
261 test value exceeds 9 °C, 1.5 PSU, respectively. Spikes in conductivity were determined by Interquartile
262 Range Test (IQR) (Hald, 1952). Quartile two and quartile three make up the interquartile range (IQR)
263 of the data. Two thresholds are defined for “suspicious” (1.5) and “bad_data” (3). The IQR is multiplied
264 by each threshold and subtracted (added) from quartile 1 (quartile 3). If a data point exceeds the
265 computed range, it is flagged accordingly. A IQR test was not applied on other variables as it was found
266 to be overly sensitive to biogeochemical variables, discarding reasonable values. Therefore, other
267 manuals and standards were used for spike detection in biogeochemical parameters.

268 Dissolved oxygen, alongside with oxygen saturation, were assessed based on the ST proposed in the
269 Manual for Real-Time Quality Control of Dissolved Oxygen Observations by the Integrated Ocean
270 Observing System (IOOS) Quality Assurance / Quality Control of Real Time Oceanographic Data
271 (QUARTOD) (IOOS QUARTOD, 2018). A spike reference (average of adjacent points DO_{n-2} and DO_n)
272 is subtracted from the tested value (D_{n-1}) and tested against an upper and lower threshold. Values failing
273 the upper boundaries are flagged as “bad_data”, values in the range of the lower and upper threshold are
274 flagged as “suspicious”. Thresholds for dissolved oxygen and oxygen saturation were set at 4 mg/l-1
275 (lower) and 8 mg/l-1(upper) and 80 % (lower) and 120 % (upper), respectively. The most reliable
276 chlorophyll-a spike detection for this dataset is proposed by The Platforms for Biogeochemical studies:
277 Instrumentation and Measure (PABIM) (PABIM, 2010). The ST algorithm remains the same as in the
278 SeaDataNet Guidelines for temperature and salinity. PABIM (PABIM, 2010) suggests an algorithm to

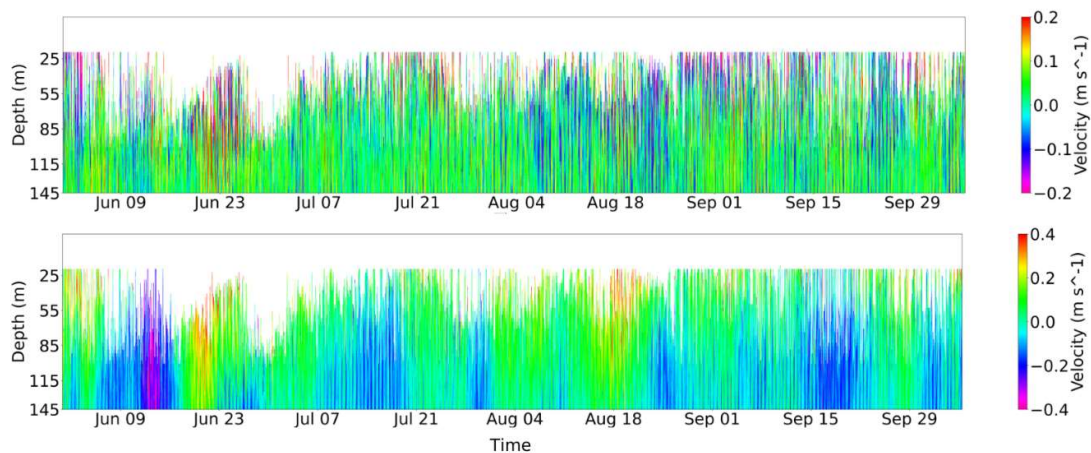
279 define the threshold value, most appropriate in any region, which is computed as follows:
 280 $\text{Threshold_Value} = |\text{median}(V_0, V_1, V_2, V_3, V_4)| + |\sigma(V_0, V_1, V_2, V_3, V_4)|$. Turbidity spikes are detected
 281 with the same methodology as chlorophyll-a, using a predefined threshold of 6 NTU.

282 6. Data Records

283 In this section we visualize the entire data series of the vertical profiles of the of the measured and
 284 derived variables in a comprehensive way. Only validated data are displayed. Data considered as bad or
 285 potentially bad were not considered to display or for the interpolations, as stated in the previous section.
 286 Preliminary analyses as well as basic statistics are presented.

287 6.1 Acoustic Doppler Current Profiler

288 Current data from the upward facing ADCP were acquired from June to October 2022 at a depth of 150
 289 m (Figure 3). Measurements above 10 m failed the quality control criteria due to interference with the
 290 surface resulting in biased data and were discarded. In the plots we present only the data below 20 m
 291 deep (Figure 3).



292

293 **Figure 3.** Meridional (north-south) (**top**) and zonal (east-west) (**bottom**) component of acoustic doppler current profiler
 294 throughout the whole water column from June to October 2022. White patches reveal absence of valid data. Negative values
 295 indicate southward (westward) flow, whereas positive values indicate northward (eastward) flow direction. Measurements are
 296 expressed in ms^{-1} . Data above approximately 20 m suffer from surface interference and were removed.

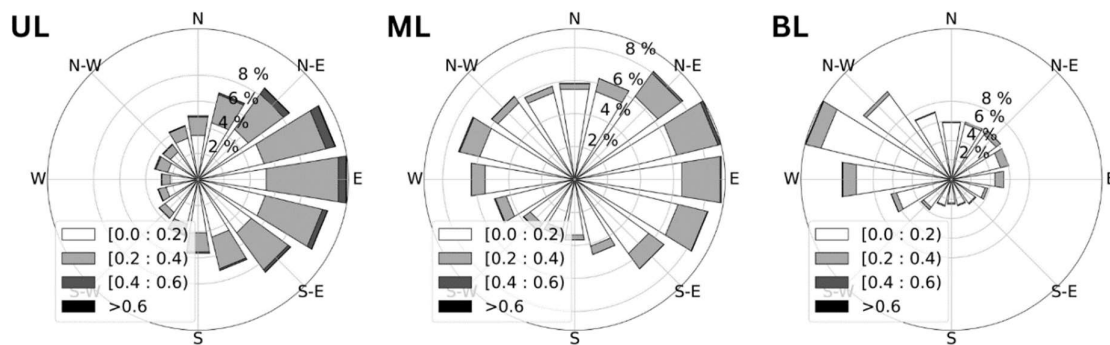
297

298 Current meter records demonstrate an energetic current regime in the area south of CSV. Clearly, the
 299 dominant flow is zonal. The meridional component is weak, without any clear tendency in the direction
 300 (notice the different scales of the velocity in Figure 3). The zonal flow shows a prevailing eastward flow,
 301 interleaved with sudden inversions to westward. Westward flows are more frequent towards the seafloor.

302 Current meter records were divided into three depth ranges to understand the distinctive current regimes
 303 along the vertical. The upper layer (UL) comprises the surface waters, reaching down to 60 m. The
 304 middle layer (ML) of the water column ranges from 60 to 100 m, and the bottom layer (BL) covers from

305 100 to 150 m. Polar plots were created for each depth layer to depict the vertical change of the magnitude
 306 and direction of the flow (Figure 4). A relatively energetic flow, showing a few episodes of increased
 307 velocities $> 0.75 \text{ m s}^{-1}$, prevails in the upper layer. There, the flow shows a strong eastward component,
 308 contrasting with the almost absence of westward flow. In the middle layer this prevalence diminishes,
 309 and the flow intensity decays, with velocities sporadically reaching values $> 0.6 \text{ m s}^{-1}$, but mostly ranging
 310 between $0.001 - 0.4 \text{ m s}^{-1}$. As we approach the seafloor, in the bottom layer, the flow is weak, with
 311 velocities between 0 and 0.2 m s^{-1} , and a prevailing westward component is evident, opposed to the
 312 upper ocean layer. A basic statistic of the flow velocity for each depth interval is presented too.

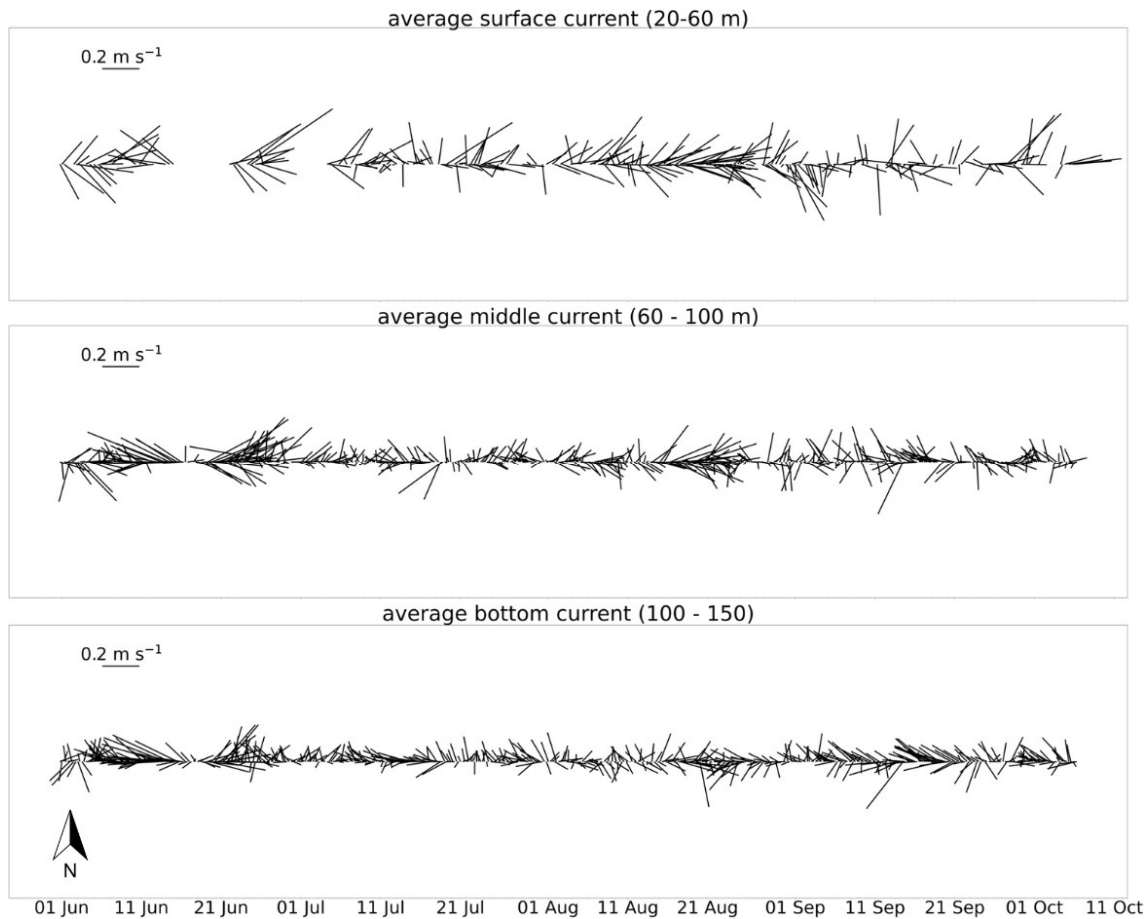
313



314

315 **Figure 4.** Demonstration of current magnitude and direction of the upper layer (UL; 10 - 60 m), middle layer (ML; 60 -
 316 100m), bottom layer (BL; 100 - 150 m).

317 To detail the temporal variability of the mean flow in each depth layer, stick diagrams are presented for
 318 each depth layer (Figure 5). The intensified current in the upper layer can be observed throughout the
 319 whole period of the deployment. A more diffuse pattern in direction, along with the decrease in velocity
 320 can be observed in the lower layers, except for a short period during mid-June. However, there is a
 321 prevalence of zonal flow, interrupted periodically by momentary direction changes. June can be
 322 identified as the most energetic month in the time series, featuring the highest mean values throughout
 323 the water column.



325

326 **Figure 5.** ADCP stick plot from June to October 2022 divided into upper layer (20-60 m; top), middle layer (60-100 m; middle)
 327 and bottom layer (100-150 m; bottom).

328 **Table 2.** Statistics of upper layer (UL; 10-60 m), middle layer (ML; 60-100 m) and bottom layer (BL; 100-150 m) grouped
 329 by month. SD representing the standard deviation. Values are expressed in ms^{-1} .

	UL				ML				LL			
	Mean	SD	Min	Max	Mean	SD	Min	Max	Mean	SD	Min	Max
June	0.247	0.105	0.009	0.773	0.186	0.095	0.004	0.574	0.142	0.080	0.001	0.687
July	0.142	0.078	0.002	0.730	0.100	0.059	0.001	0.787	0.089	0.047	0.000	0.509
August	0.182	0.096	0.001	0.639	0.125	0.074	0.000	0.469	0.098	0.053	0.001	0.385
Sept	0.151	0.096	0.003	0.716	0.107	0.059	0.001	0.600	0.101	0.058	0.002	0.510

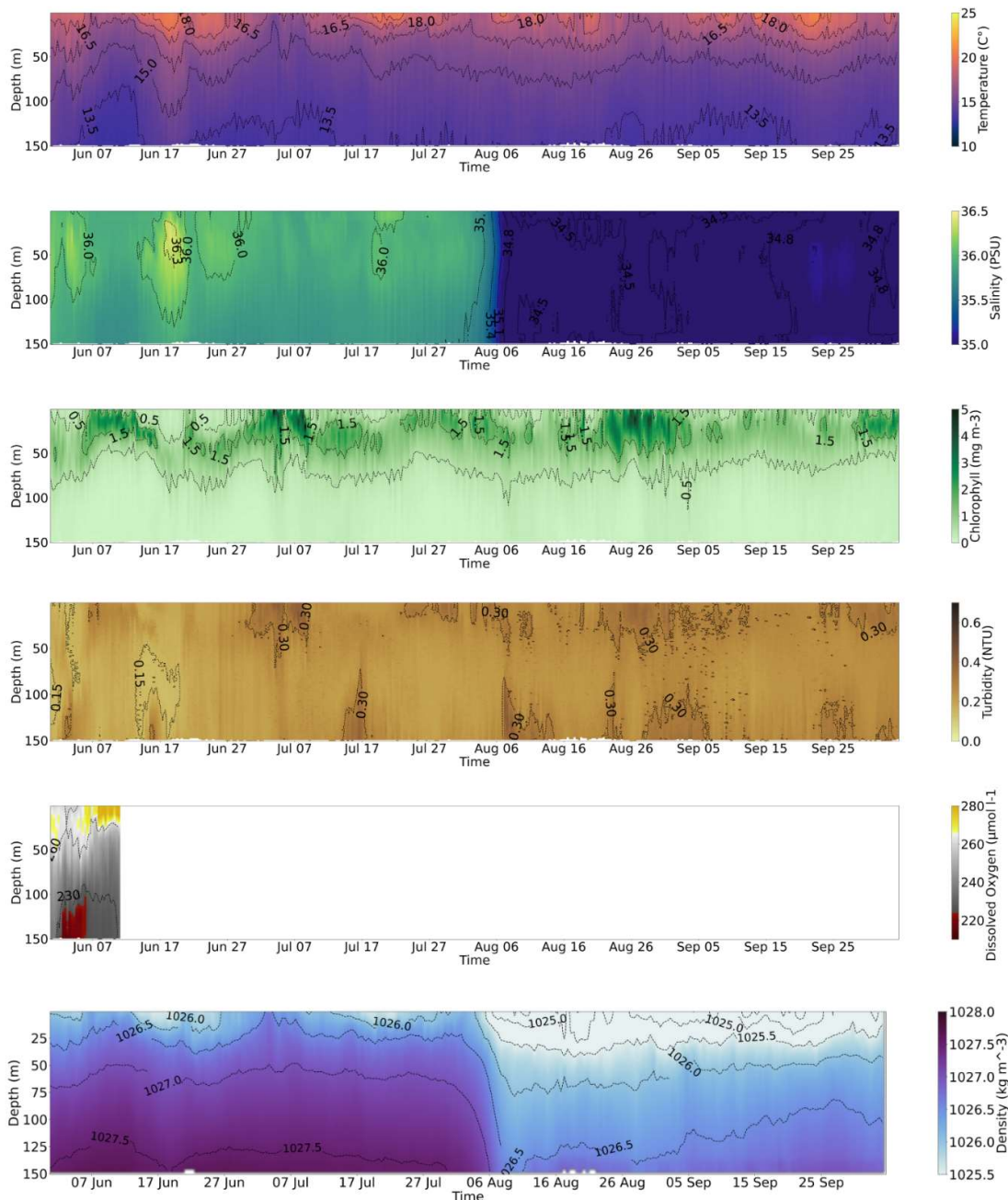
330

6.2 Vertical wave-powered profiler

331

Continuous time series of the entire water column are highly valuable as they offer vast amounts of data
 332 and can create a comprehensive picture of mesoscale and sub-mesoscale processes. The vertical wave-
 333 powered profiler, equipped with physical and biogeochemical sensors, operated for four months
 334 continuously, and delivered a rich dataset at the end of the deployment. Vertical profiles of the water
 335 column show temperatures between $12.5 \text{ }^\circ\text{C}$ closer to the seafloor to approximately $22 \text{ }^\circ\text{C}$ on the surface
 336 (Figure 6; Table 3). The thermocline remains between 20-40 m, showing some periods of a well-mixed
 337 homogenous surface layer and periods of more stratified waters (Figure 6; Figure 7). Salinities are found

338 to range between 33 and 37 from June to the end of July with an average salinity of 35.95 (SD \pm 0.13)
339 and 35.88 (SD \pm 0.09), respectively (Figure 6; Table 3). Salinity data beyond that point were discarded
340 and will not be discussed further as the conductivity sensor was subject to intense biofouling, prohibiting
341 the collection of trustworthy measurements after the month of July. Due to that the mixed layer depth
342 was only computed for the months of June and July, showing an average Mixed-Layer Depth (MLD)
343 around the 10-20 m mark, following the pattern of the thermocline (Figure 8, top). The dissolved oxygen
344 sensor shows lower oxygenated waters in deeper waters but stopped operating after two weeks
345 (Figure 6). The chlorophyll-a maximum can be found between 20-60 m with concentrations between
346 1-10 mg m⁻³ and mitigates to almost 0 mg m⁻³ below (Figure 6; Figure 7; Table 3). Turbidity
347 concentrations correspond to chlorophyll-a during the whole course of the measurements, with average
348 concentrations of 0.25 NTU (SD \pm 0.17), indicating the correlation between turbidity and biomass with
349 some additional phases of increased turbidity concentrations close to the seafloor (Table 3).



351

352 **Figure 6.** Continuous vertical wave profiler data Jun-Oct 2022. **Top to bottom:** Temperature ($^{\circ}\text{C}$), salinity, chlorophyll-a
 353 concentration (mg m^{-3}), turbidity (NTU), dissolved oxygen ($\mu\text{mol l}^{-1}$), and density (kg m^{-3}). Salinity and density values after
 354 the month of July are ambiguous and are discarded from further discussion.

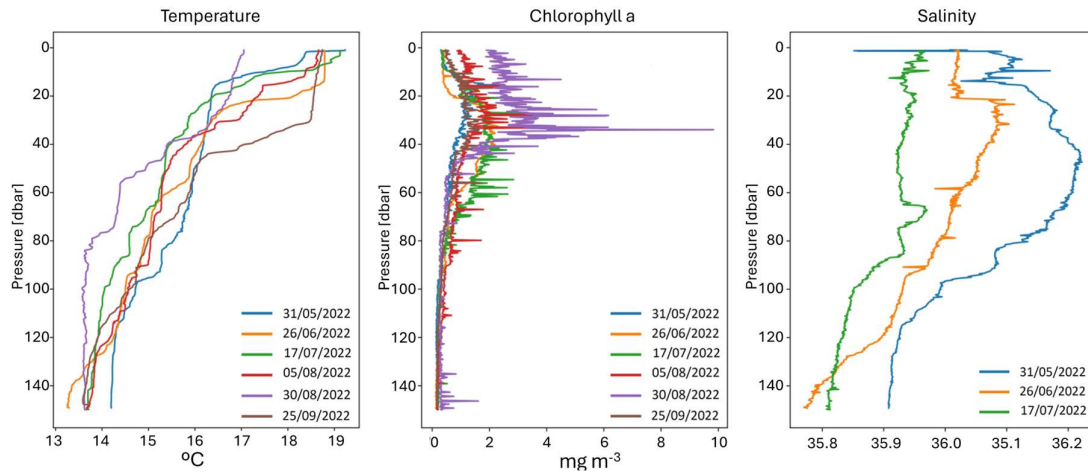
355 In June two period of increased salinity were recorded between the 1st – 6th and 13th to the 21st of June
 356 near the surface down to 120 m depth, together with mitigation in chlorophyll-a concentration, migrating
 357 to deeper layers along the mixed layer to a depth of approximately 60 m (Figure 6; Figure 8). The salty
 358 waters appear in form of an isolated lens, carrying maximum salinities of 36.72 (Figure 6; Figure 7).
 359 Simultaneously, an intensification in stability and spiciness can be observed (Figure 8). Spiciness was

360 computed with the Thermodynamic Equation of Seawater 2010 (TEOS-10) from Absolute Salinity and
 361 Conservative Temperature, according to McDougall and Krzysik (2015).

362 Table 3. Statistics of vertical wave-powered profiler parameters grouped by month. SD representing the standard deviation.
 363 Recordings are lacking for the variables dissolved oxygen, oxygen saturation after the first half of June and for salinity after
 364 July.

	June				July			
	Mean	SD	Min	Max	Mean	SD	Min	Max
Temperature (°C)	15.55	1.97	12.62	21.3	15.15	1.7	12.64	20.51
Conductivity (S m ⁻¹)	4.46	0.21	4.13	5.06	4.41	0.18	4.14	4.98
Salinity	35.95	0.13	34.44	36.72	35.88	0.09	34.13	37.02
Dissolved Oxygen (µmol l ⁻¹)	245.35	18.5	209.96	305.46	-	-	-	-
Oxygen Saturation (%)	97.77	10.5	81.08	120.0	-	-	-	-
Chlorophyll a (mg m ⁻³)	0.59	0.65	0.08	9.33	0.76	0.81	0.09	10.84
Turbidity (NTU)	0.2	0.07	0.0	6.17	0.25	0.09	0.0	6.42
Sound velocity (m s ⁻¹)	1510.48	5.43	1502.08	1526.23	1509.22	4.62	1502.31	1524.2
	August				September			
	Mean	SD	Min	Max	Mean	SD	Min	Max
Temperature (°C)	15.41	1.64	12.64	21.56	15.48	2.03	12.74	21.22
Conductivity (S m ⁻¹)	4.31	0.16	4.01	4.88	4.32	0.19	4.02	4.90
Salinity	-	-	-	-	-	-	-	-
Dissolved Oxygen (µmol l ⁻¹)	-	-	-	-	-	-	-	-
Oxygen Saturation (%)	-	-	-	-	-	-	-	-
Chlorophyll a (mg m ⁻³)	0.83	0.88	0.09	10.51	0.61	0.58	0.08	9.40
Turbidity (NTU)	0.27	0.10	0.04	7.13	0.27	1.41	0.03	363.77
Sound velocity (m s ⁻¹)	1508.76	4.35	1500.69	1524.31	1508.89	5.44	1501.0	1524.69

365
 366 Throughout the first half July colder and less saline waters shoal towards the surface with average values
 367 of 14.83 ± 1.44 °C and 35.87 ± 0.07 , respectively (Figure 6), resulting in a well-mixed and homogenous
 368 water column. In response, stability and spiciness decrease (Figure 8), accompanied by increasing
 369 chlorophyll-a concentration (0.9 ± 1.03 mg m⁻³) and turbidity (0.26 ± 0.07 NTU). In the second half of
 370 the months surface waters experience warming and average increase slightly up to 15.40 ± 1.83 °C,
 371 along with an increased stability and spiciness (Figure 6; Figure 8). Stratification enhances during
 372 August due to a deepening of the warmer surface waters to a depth of approximately 60 m (Figure 8).
 373 Around the 24th of August colder temperate waters shoal towards the surface (19.4 °C), simultaneously
 374 with an inflation of the maximum chlorophyll-a concentration (10.51 mg m⁻³), attenuating in the
 375 beginning of September. Upper layer stratification stabilizes throughout the month of September, with
 376 temperatures around 21 °C in the upper 40 m with an increased period of warming between the second
 377 and third week of the month along with a slight decrease of chlorophyll-a (Figure 6). The same pattern
 378 was observed during mid-August, in which, with increased surface temperatures, higher chlorophyll-a
 379 concentrations migrate to deeper layers, similar to the third week of July.

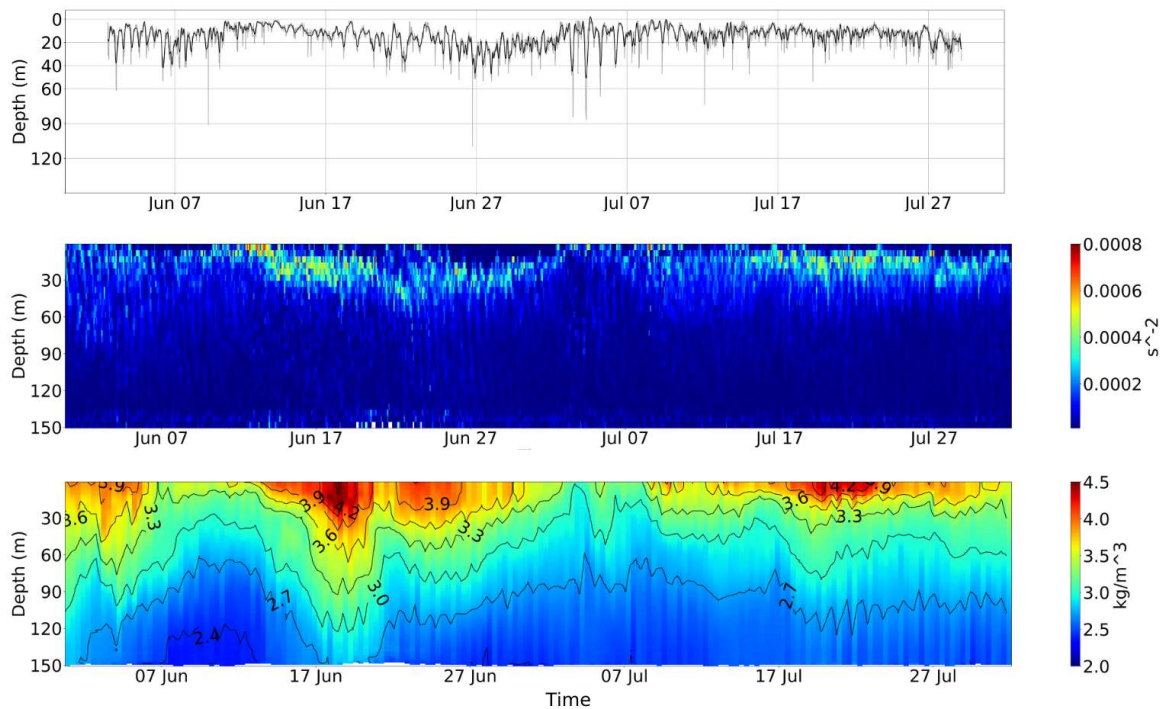


380

381

382

Figure 7. Examples of individual vertical profiles of temperature (°C) (**left**), chlorophyll-a (mgm-3) (**middle**) and salinity (**right**).



383

384

385

Figure 8. From **top to bottom**: MLD, Brunt-Väisälä frequency (N^2), spiciness. Computed for the months of June and July. Subsequent failure of conductivity sensor prohibits computation of presented parameters from that point on.

386

7. Data availability

387

388

389

390

391

392

Quality controlled datasets are made publicly available as NetCDF files at the environmental data repository SEANOE (<https://www.seanoe.org/>) under the DOI <https://doi.org/10.17882/94769> in accordance with FAIR principles (Wilkinson et al., 2019). Beyond the repository, data is ingested into the CCMAR Erddap server (<https://erddap.cmar.ualg.pt/erddap/index.html>), in which a first data visualization and data can be downloaded in various file formats selectively from the user. Further, the data is shared with the EMSO-ERIC Data Portal (<https://data.emso.eu/home>), in which users can

393 visualize and download data according to their needs. The data is not restricted and is accessible for
394 anyone, accompanied with comprehensive metadata. Standardized datasets allow machine readability
395 and interoperability with various software.

396 **8. Data set value**

397 This dataset conveys the importance of continuous, long-term data acquisition and ocean monitoring to
398 capture mesoscale and sub-mesoscale events in the ocean. As presented before it was detected, for
399 example during the second half of June, fascinating thermohaline records. This deployment was the first
400 test run of the IbMa-CSV Ocean Observatory. Sensor failure due to biofouling will be tackled by
401 following a regular cleaning of the sensors at specific time intervals while deployed (profiler), and by
402 reducing deployment turn-around with a second vertical wave-powered profiler. Hence, the two profilers
403 will alternate in a minimum four month rhythm, therefore guarantying a continuous data collection. The
404 vertical wave-powered profiler offers impeccable high temporal and vertical resolution data products at
405 reasonable cost and maintenance. The only instruments which provide data products with comparable
406 resolution are autonomous underwater vehicles and gliders. Yet both economically and regarding the
407 scope of establishing an Eulerian, long-term observation platform, these instruments cannot compete,
408 underpinning the exceptional potential of the vertical wave-powered profiler and its data products.

409 The monitoring of energetic areas, such as the western tip of the northern margin of the Gulf of Cadiz
410 (the CSV), is crucial to understand the complexity of the ocean dynamics and to predict future
411 development via ocean models and their validation through comprehensive datasets. A wide range of
412 processes, from the upper layers wind induced upwelling to deeper MOW features, do occur in the ocean
413 surrounding CSV, as described in the Introduction. Intense mesoscale and sub-mesoscale activity, that
414 represent the “weather” variability of the ocean imposed by the turbulent nature of the circulation, are
415 quite conspicuous in this region and dominates all levels of the water column, challenging the
416 investigation of a wide range of oceanographic processes.

417 Efforts have been made to develop numerical models for this region, with the aim of better
418 understanding the exchange and mixing processes that occur there, and their implications for the
419 ecosystem and salt spreading in the North Atlantic. However, there is no general theory of turbulence,
420 and numerical models must rely on parametrizations to solve this macro-turbulence. The correct
421 parameterization of the turbulent behavior of the ocean depends on the previous knowledge that we have
422 about the physical characteristics of the region to be modelled. This knowledge is built upon the
423 observation of the ocean. Higher resolution observations will produce better parameterizations of the
424 numerical models. The present knowledge of the oceanography of the region is inferred from event scale
425 sampling, leading to regional numerical models highly data deficient., that tend to use parameterization
426 analogies with ocean regions with similar oceanographic characteristics and intensively sampled, such
427 as the California Upwelling System (Macias et al., 2014; Janeiro et al., 2017). This data series will make

428 it possible to find better parameters for the region and to solve more realistically the turbulence and
429 turbulence related ocean processes.

430 The present data set, with such vertical and temporal resolution, is unique in the region. The nearest
431 moorings, operated by the Instituto Hidrográfico (Portugal), are more than 120 km away, and only take
432 measurements at the surface (<https://www.hidrografico.pt/index/en>). The velocity field is assessed only
433 at the surface through HFRs that cover the region, operated by the Puertos del Estado (Spain)
434 (<https://www.puertos.es>) and the Instituto Hidrográfico (Portugal). For the first time the subsurface is
435 sampled in the region. The high-resolution sampling, covering the surface layer down to a depth of 150
436 meters, makes this dataset unique in a vast area of the ocean, disclosing the high oceanographic value
437 of the data set. The IbMa-CSV Ocean Observatory was established in the scope of EMSO-ERIC, a
438 European wide ocean observatory network, and will be further developed and improved to operate
439 continuously and long-term.

440 **9. Usage note**

441 EMSO data are published without any warranty, express or implied. The user assumes all risk arising
442 from the use of EMSO data. EMSO data are intended to be research-quality and include estimates of
443 data quality and accuracy, but it is possible that these estimates or the data themselves contain errors. It
444 is the sole responsibility of the user to assess if the data are appropriate for his/her use, and to interpret
445 the data, data quality, and data accuracy accordingly. EMSO welcomes users to ask questions and report
446 problems to the contact addresses listed in the data files or on the EMSO web page.

447 **10. Acknowledgement**

448 This study received Portuguese national funds from: FCT - Foundation for Science and Technology
449 through project UIDB/04326/2020, UIDP/04326/2020 and LA/P/0101/2020; operational programmes
450 CRESC Algarve 2020 and COMPETE 2020 through projects EMBRC.PT ALG-01-0145-FEDER-
451 022121 and EMSO-PT ALG-01-0145-FEDER-022231; EEA Grants Blue Growth project "Atlantic
452 Observatory – Data and Monitoring Infrastructure" (PT-INNOVATION-0002). Furthermore, we would
453 like to acknowledge and thank the R/V Mário Ruivo for the ship-time and support of the crew. The
454 authors would like to acknowledge that the research for this study was conducted at the Centre of Marine
455 Sciences (CCMAR), University of Algarve, Faro, Portugal and the Portuguese Institute for the Sea and
456 Atmosphere (IPMA, I.P.), Lisboa, Portugal.

457 **11. Author Contribution**

458 CS designed the instrument setup and the deployment strategy. SR, PR, CS, MC carried out the
459 equipment deployment and recovery. SA did the data processing, harmonization and publishing. SR,
460 PR, CS prepared the paper, with contributions from all co-authors.

461 **12. Competing Interests**

462 The contact author has declared that none of the authors has any competing interests.

463 **References**

- 464 Ambar I., A shallow core of Mediterranean water off western Portugal. *Deep-Sea Res* 30(6A):677-
465 680, 1983.
- 466 Ambar, I., Serra, N., Neves, F., and Ferreira, T., Observations of the Mediterranean Undercurrent and
467 eddies in the Gulf of Cadiz during 2001, *J. Mar. Sys.*, 71, 195–220, 2008.
- 468 Aristegui, J., Álvarez-Salgado, X., Barton, E., Figueiras, F., Hernández-León, S., Roy, C., Santos, A.,
469 Oceanography and fisheries of the Canary Current/Iberian region of the eastern North Atlantic. In:
470 Robinson, A., Brink, K. (Eds.), *The Sea, In: The Global Coastal Ocean: Interdisciplinary Regional*
471 *Studies and Syntheses*, vol. 14 (Part B). Harvard University Press, Cambridge, MS, pp. 877–931,
472 2006.
- 473 Bower, A., L. Armi, and I. Ambar, Direct evidence of meddy formation off the southwestern coast of
474 Portugal. *Deep-Sea Res.*, 42, 1621–1630, 1995.
- 475 Cardeira S., F. Rita, P. Relvas, A. Cravo, Chlorophyll *a* and chemical signatures during an upwelling
476 event off the South Portuguese coast (SW Iberia). *Continental Shelf Research* 52, 133–149. 2013.
477 <http://doi.org/10.1016/j.csr.2012.11.011>
- 478 Coppola, L., Ntoumas, M., Bozzano, R., Bensi, M., Hartman, S. E., CharcosLlorens, M. I., et al. (2016).
479 Handbook of Best Practices for Open Ocean Fixed Observatories. European Commission, FixO3
480 Project, 127. (European Commission, FixO3 project, FP7 Programme 2007-2013 under grant
481 agreement n° 312463). Available online at: <http://hdl.handle.net/111penalty-\@M329/302>
- 482 Garel, E.; Laiz, I.; Drago, T.; Relvas, P., Characterisation of coastal counter-currents on the inner shelf
483 of the Gulf of Cadiz. In: *Journal of Marine Systems* 155, S. 19–34., 2016
- 484 Hald, A., *Statistical theory with engineering applications*, John Wiley Sons, New York, ISBN-10
485 0471340561, 1952.
- 486 IOOS QUARTOD, Manual for Real-Time Quality Control of Dissolved Oxygen Observations,
487 Version 2.1, August, 2018,
488 https://cdn.ioos.noaa.gov/attachments/2018/08/QARTOD_DOSecondUpdate_final.pdf, (last access:
489 27 March 2023)
- 490 Janeiro, J., Neves, A., Martins, F., and Relvas, P., Integrating technologies for oil spill response in the
491 SW Iberian coast, *Journal of Marine Systems*, Volume 173, 31-42, 2017.
- 492 Macias, D. M., Guerreiro, C. T., Prieto, L., Peliz, A. and Ruiz, J., A high-resolution hydrodynamic-
493 biogeochemical coupled model of the Gulf of Cadiz – Alboran Sea region”, *Mediterranean Marine*
494 *Science*, 15(4), pp. 739–752, 2014.
- 495 Mauritzen C., Morel Y., Paillet J., On the influence of Mediterranean water on the central waters of
496 the North Atlantic Ocean , *Deep-Sea Research I*, vol. 48 (pg. 347-38), 2001.
- 497 McDougall, T. J., & Krzysik, O. A., Spiciness, *Journal of Marine Research*, 73(5), 141–152. 2015.
498 <https://doi.org/10.1357/002224015816665589>
- 499 OceanSITES, Data Format Reference Manual, Version 1.4. ,2020.
500 http://www.oceansites.org/docs/oceansites_data_format_reference_manual.pdf (last access: 27 March
501 2023)

502 PABIM (Platforms for Biogeochemical studies: Instrumentation and Measure), White book on oceanic
503 autonomous platforms for biogeochemical studies: Instrumentation and measure, Version 1.3,
504 February 2010.
505 [https://www.coriolis.eu.org/content/download/3150/23513/file/2009_PABIM_white_book_version1.3.](https://www.coriolis.eu.org/content/download/3150/23513/file/2009_PABIM_white_book_version1.3.pdf)
506 [pdf](https://www.coriolis.eu.org/content/download/3150/23513/file/2009_PABIM_white_book_version1.3.pdf), (last access: 27 March 2023)

507 Rautenbach Sarah, Relvas Paulo, Sousa Carlos (2022). EMSO-Iberian Margin Cape St. Vincent
508 observatory data (subsurface mooring) from Jun-Oct 2022. SEANO. <https://doi.org/10.17882/94769>

509 Relvas, P., and E.D. Barton, Mesoscale patterns in the Cape São Vicente (Iberian Peninsula) upwelling
510 region, *Journal of Geophysical Research*, 107(C10), 3164, doi:10.1029/2000JC000456, 2002.

511 Relvas, P., and E. D. Barton, A separated jet and coastal counterflow during upwelling relaxation off
512 Cape São Vicente (Iberian Peninsula), *Continental Shelf Research*, 25, 29-49, 2005.

513 Sánchez-Leal, R.F., M. J. Bellanco, L. M. Fernández-Salas, J. García-Lafuente, M. Gasser-Rubinat, C.
514 González-Pola, F. J. Hernández-Molina, J. L. Pelegrí, A. Peliz, P. Relvas, D. Roque, M. Ruiz-
515 Villarreal, S. Sammartino, J. C. Sánchez-Garrido, The Mediterranean Overflow in the Gulf of Cadiz:
516 A rugged journey. *Sci. Adv.* 3, eaao0609 (2017) <https://doi.org/10.1126/sciadv.aao0609>

517 SeaDataNet, Data Quality Control Procedures, 6th Framework of EC DG Research, Version 2.0, May
518 2010, <https://www.seadatanet.org/Standards/Data-Quality-Control> (last access: 27 March 2023)

519 Serra N, Ambar I, Boutov D, Surface expression of Mediterranean Water dipoles and their
520 contribution to the shelf/slope–open ocean exchange. *Ocean Sci* 6:191–209, 2010.

521 Wilkinson, M. D., Dumontier, M., Appleton, G., Axton, M., Baak, A., Blomberg, N., et al. (2019).
522 Addendum: the FAIR guiding principles for scientific data management and stewardship. *Sci. Data* 6:6.
523 doi: 10.1038/s41597-019-0009-6

524